Journal of Marine Science and Technology

Volume 11 | Issue 1 Article 1

Empirical Orthogonal Function Analysis of AVHRR Sea Surface Temperature Patterns in Taiwan Strait

Ming-An Lee
Department of Environmental Biology and Fisheries Science, National Taiwan Ocean University, Keelung 20224, Taiwan, Republic of China., malee@mail.ntou.edu.tw

Ching-Dong Yeah
Department of Environmental Biology and Fisheries Science, National Taiwan Ocean University, Keelung 20224, Taiwan, Republic of China.

Chao-Hsiung Cheng
Department of Environmental Biology and Fisheries Science, National Taiwan Ocean University, Keelung 20224, Taiwan, Republic of China.

Jui-Wen Chan
Department of Environmental Biology and Fisheries Science, National Taiwan Ocean University, Keelung 20224, Taiwan, Republic of China.

Kuo-Tien Lee
Department of Environmental Biology and Fisheries Science, National Taiwan Ocean University, Keelung 20224, Taiwan, Republic of China.

Empirical Orthogonal Function Analysis of AVHRR Sea Surface Temperature Patterns in Taiwan Strait

Acknowledgements

We would like to express our appreciation to Mr. I.M. Chen and M.S. Chou for their assistance on SST imageries extracted and the EOF analysis, respectively. The study was financially supported by the National Science Council (NSC 89-2611-M-019-02-04-op4 and NSC 89-2119-M019-004) of the Republic of China (R.O.C).

EMPIRICAL ORTHOGONAL FUNCTION ANALYSIS OF AVHRR SEA SURFACE TEMPERATURE PATTERNS IN TAIWAN STRAIT

Ming-An Lee, Ching-Dong Yeah, Chao-Hsiung Cheng, Jui-Wen Chan, and Kuo-Tien Lee

Key words: AVHRR, SST, Taiwan Strait, EOF.

ABSTRACT

Empirical orthogonal function (EOF) analysis was used to study a time-series of the Advanced Very High Resolution Radiometer (AVHRR) imageries from the waters of Taiwan Strait to examine the temporal and spatial characteristics and to determine the dominant pattern of sea surface temperature (SST) variability for 72 months from January 1996 to December 2001. The spatial variance was consistent with a quasi-permanent front at the Chang-Yuen Ridge in winter and associated with strong temperature contrast to the Kuroshio branch or the South China Sea Warm Current. It also displayed a cool water plume extending from the Peng-Hu Islands to Formosa Banks in summer. The EOF patterns and the eigenvalues in time and space were similar to each other. The dominant EOF mode, which resembled the mean of all images, showed a crescentic-shaped front near the Chang-Yuen Ridge where a cool tongue extending from China Coastal Waters was distinguishable from the warm current. The second mode revealed that the South China Sea Warm Current and the Taiwan Warm Current were over the Peng-Hu Channel following the 60- to 100-m isobaths. These two spatial modes accounted for 69.51% and 8.78% of the SST variance, respectively. From these images, we also discussed the characteristics of the SST variance in relation to the environments in winter.

INTRODUCTION

With an increasing availability of satellite sea surface temperature (SST) and ocean color data, it has become possible to monitor temporal and spatial variation in both SST and chlorophyll-a. These data improve greatly from the very limited spatial data offered by ship observations. Generally, there are routine archives that have been used to analyze time-series of measurements of some parameters, such as SST variability [5, 11, 12, 21], currents [5], fronts [6, 10], eddies [19] or some special indices associated with fishery oceanography [1, 4, 17]. Among the methods available, the empirical orthogonal function (EOF) analysis has been a particularly useful tool in studying large quantities of multivariate data [5, 11, 14]. This method decomposes a time-series data set into its orthogonal component modes, of which the first few can be used to describe the dominant patterns of variance in the time-series.

The Taiwan Strait is located at the confluence of the East China Sea and the South China Sea in the west Pacific Ocean between Taiwan and Mainland China (Figure 1). A distinct special topographic feature in the strait is the Chang-Yuen Ridge, extending westward from the middle of the west coast of Taiwan. It separates the strait into two basins and builds a boundary for the ocean circulation for China Coastal Water, South China Sea Warm Current and Taiwan Warm Current in

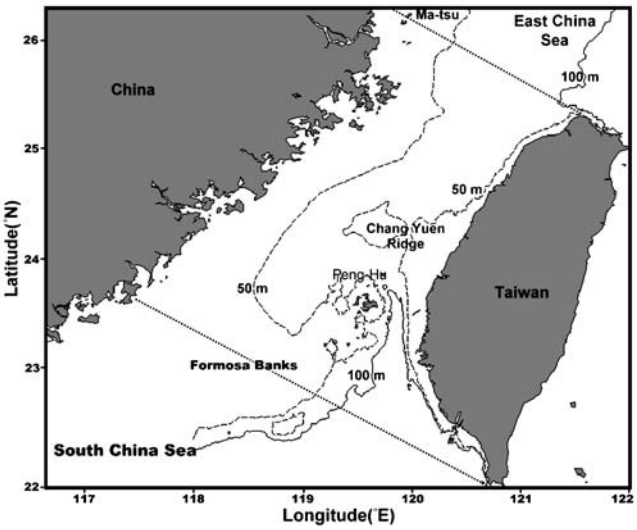

Fig. 1. Location of the Taiwan Strait. The dotted lines indicated the boundaries of the sample area for AVHRR SST imageries in this study. The dashed and solid lines show the isobaths of 50 m and 100 m, respectively.

Paper Submitted 05/07/02, Accepted 12/17/02. Author for Correspondence: Kuo-Tien Lee.
Department of Environmental Biology and Fisheries Science, National Taiwan Ocean University, Keelung 20224, Taiwan, Republic of China. E-mail: malee@mail.ntou.edu.tw.

winter and summer [7, 8]. Another important feature of both Peng-Hu Islands and Formosa Banks is their locations at the south of the strait. It is a shallower water less than 40 m deep. Between them, the Peng-Hu Channel, a submarine channel deeper than 60 m, induces the mean current move northward from South China Sea to East China Sea. Both waters and biogeochemical flux of the East China Sea and the South China Sea are exchanged through the strait. It is difficult to monitor their near-real time hydrographic features by using the hydrological model with the *in situ* observations, because the observation data less than 30 m deep from the survey vessel can not routinely be obtained. Liao et al. [15] indicate that AVHRR SST obtained from satellite differs about 0.21°C from surface sea temperature obtained from ship survey for the water of Taiwan. In this study, we used the EOF method to decompose a time-series of 72-month SST images of the Taiwan Strait into component modes of oscillation.

MATERIALS AND METHODS

1. Satellite SST images

The raw satellite images of Taiwan Strait were collected from the Advanced Very High Resolution Radiometer (AVHRR) on the NOAA 12, 14, 15 and 16 satellites and archived by the Department of Environmental Biology and Fishery Sciences, National Taiwan Ocean University. The images were received about four to six times per days during the period of January 1996 to December 2001. All satellites images were navigated (i.e. corrected for distortion and registered to a map), and were nudged (i.e., entire imaged shifted to fit map overlap) to correct for receiving system timing errors or satellite altitude errors. The ground resolution was 1.1 Km at nadir. The navigation and cloud detection techniques used in this study were described by Emery et al [2]. Among them, the cloud-free images were further processed to obtain the multi-channel sea surface temperature data [13,18]. A total of 3179 daily AVHRR images were collected from January 1996 to December 2001. Monthly SST data were formed by arithmetically averaging all available scenes in each month on a pixel by pixel basis (excluding missing data and clouds).

The study area (Figure 1) was about 360 km alongshore by 160 Km offshore. For the convenience of computation and analysis, we averaged the SST data per 5 pixels, so that the SST spatial resolution changed from original 1.1 Km by 1.1 Km to 5.5 Km by 5.5 Km. There were 2631 spatial data points per month over the study area. The 72 (6 years) monthly data were arranged into a two-dimensional array $T(x, t)$, where x and t were the spatial and temporal indices, respectively.

2. EOF analysis

EOF analysis is a statistical method used to decompose a multi-variate data set into its principal components. Using this method, the bulk of the variance of a data set can be described by a few orthogonal modes, so that the major properties of the data set can be more easily understood. As applied in this research, the original multi-variate data set was a time series of SST imageries which had two spatial dimensions and one temporal dimension. In order to obtain the two dimensional matrix for the analysis, the columns of each image were stacked so that the image became a column vector. When these column vector images were placed together as sequential column, an $M \times N$ matrix, $T(x, t)$, was formed, where M is the number of elements in the spatial dimension, in this case the number of pixels in an image, and N is the number of elements in the temporal dimension, in the case the number of images. Generally, the time-series of images can be represented by a linear combination of the eigenfunction (F_n) as equation (1):

$$T(x, t) = \sum_{n=1}^{N} a_n(t) F_n(x) \tag{1}$$

where a_n is the temporal amplitude or eigenvector. The eigenfunctions, or spatial amplitude functions, can themselves be viewed as images, giving a visual representation of the variance of each mode.

In order to extract more detail information from EOF analysis, Paden *et al* [16] suggest that temporal and spatial demeaning of the data matrix is performed before EOF analysis. The removal of the temporal and spatial means revealed features that vary strongly in time and space, respectively. The temporal mean was removed by finding the mean over the time-series at each pixel (i.e. in each row of $T(x, t)$), and then subtracting the mean from each pixel in that row (Equation 2).

$$T'_t(x, t) = T(x, t) - \frac{1}{N} \sum_{t=1}^{N} T(x, t) \tag{2}$$

The spatial mean was removed from $T(x, t)$ by calculating the mean of each image (column of $T(x, t)$), and subtracting it from each pixel in that image (Equation 3).

$$T'_s(x, t) = T(x, t) - \frac{1}{M} \sum_{x=1}^{M} T(x, t) \tag{3}$$

The amplitude scores were estimated by the formula: $Z_t(x) = Z'(x, t) \times \sum_{t=1}^{N} a_n(t)$, where $Z_t(x)$ is the amplitude score of pixel x; a_n is the eigenvector; $Z'(x, t)$ is the standardized value of the data matrix $T(x, t)$ and N is the number of images.

Finally, both the temporal and spatial amplitude

scores of $T'(x, t)$ SST images were used to decompose the data matrix by using the singular value decomposition (SVD) method for elucidating the spatial and temporal patterns of sea surface temperature in Taiwan Strait.

RESULTS

1. Monthly mean sea surface temperature

Figure 2 shows the monthly mean surface temperature of Taiwan strait derived from the AVHRR of NOAA-12, 14, 15 and 16 for the period of January 1996 to December 2001. Beginning with the northeast monsoon in October to November, a cold surface water of 22 to 25°C reached to the west side of the Taiwan Strait. In December a cold tongue of surface water, with temperature between 15°C and 18°C, extended southwestward from the East China Sea near to the waters of the Chang-Yuen Ridge. South of this cold tongue, SST gradually increased with warmest water (>24°C) found near the southwest coast of Taiwan. Cold SST along the coast of the mainland during the northeast monsoon was a result of evaporative cooling from the flow of cold continental air over the water, and was further enhanced by the entrainment of subsurface water by a turbulence generated by surface cooling. However, this cold tongue was restricted at the boundary of the Chang-Yuen Ridge by the warmer water.

From April this cold tongue gradually weakened and moved northward and was replaced by a belt of warm surface water with temperature between 28°C and 31°C. During the transition from northeast monsoon to southwest monsoon, the 29°C and warmer SST were over most of the Taiwan Strait. Around the beginning of June, the area of above 29°C water intruded northward and eastward. A cold pocket of surface water was seen in the waters surrounding the south coast of the Peng-Hu islands. The formation of these cold pockets was attributable to upwelling. These cold wedges appeared with regularity and at about the same locations from June to September in the satellite SST imageries, and the warm surface water rapidly replaced the cold water along the coast of the mainland. This trend persisted until October when the cooling associated with the northeast monsoon began to take effect, starting with formation of cold SST near the coast of Mainland China which then propagated southwestward.

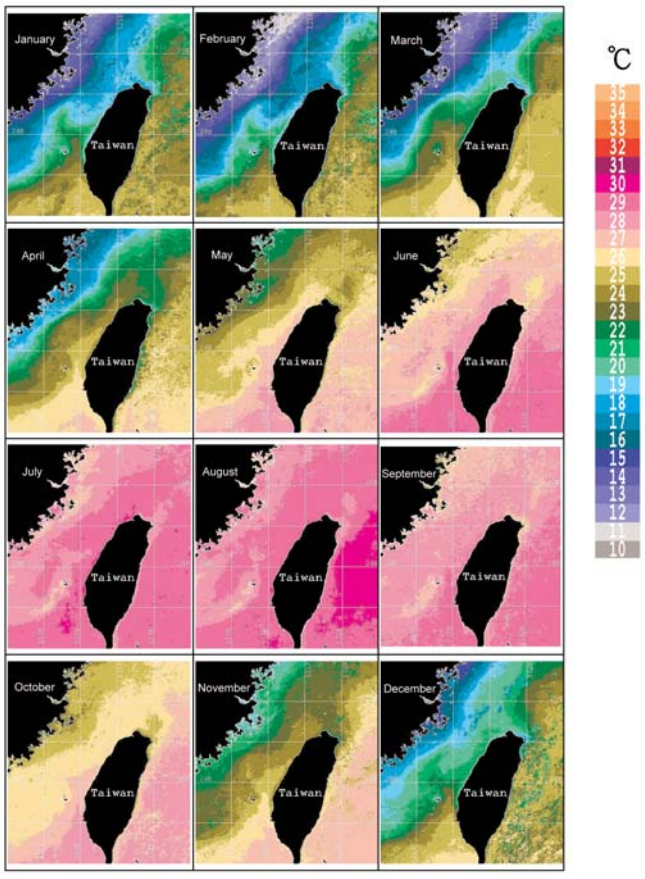

Fig. 2. The monthly mean sea surface temperature imageries derived by AVHRR of NOAA 12, 14, 15 and 16.

2. Eigenvalues features

The eigenvalues for both the spatial and temporal variance EOFs are graphically shown in Figure 3. The first mode was heavily dominant in both cases, and a very steep drop in variance follows for the next few modes. The drop-off was most dramatic for the covariance variance analysis, where the first and second modes accounted for 62% and 8.59% of the total variance,

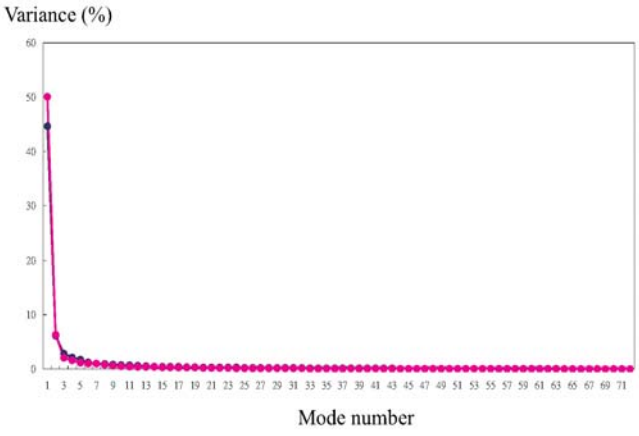

Fig. 3. EOF eigenvalues of the 1996 to 2001 monthly satellite SST imagery data set for the temporal variance (blue color) and spatial variance (pink color).

respectively. This indicated that there was a strong time-varying signal in the data which virtually overwhelmed any other temporal variability. By contrast, the first and second spatial variance modes were 69.51% and 8.78%, respectively. The change in variance between the first and second spatial variance modes is also very large, indicating that the surface temperatures in the strait were dominated by a unique spatial pattern. It implied that the eigenvalues in temporal and spatial variances were similar to each other.

3. Temporal and spatial variance

Figure 4 and 5 show the eigenvectors and the spatial amplitude functions for the first two temporal and spatial variances, respectively. The first covariance modes accounted for 62% of the sea surface temperature variability. The spatial amplitudes were all positive in the waters of Taiwan Strait. Since the spatial amplitude was positive, a positive eigenvector represented a sea surface temperature above the mean for the time-series. The time series began in January 1996, when the sea surface temperatures were colder and the eigenvector was negative. This mode illustrated patterns associated with the dominated seasonal cycle in the SST variance. The second covariance mode made up 8.59% of total variance. The spatial amplitudes of mode 2 were all negative, being constant zero in the middle part of the strait, with slightly larger negative value in the coastal waters.

The first spatial mode made up 69.51% of the total spatial variance. It was similar to the pattern of temporal EOF mode 1. The spatial amplitudes for this mode ranged from negative value near to the coast of Mainland China, to positive value in the southeast of the study area. The second spatial mode accounted for 8.78% of total spatial variance. The spatial amplitude patterns had positive values in the coastal waters of Mainland China. The spatial amplitudes of the deeper waters up to the middle of the straits remained near zero or negative values.

Figure 6 shows the power spectrum of the eigenvector in the temporal and spatial time-series EOF analysis. The power spectrum showed that the temporal and spatial mode 1 was mostly constant at a frequency of 12 months, with a weak peak at a period of 7 months in spatial mode. The variance analysis of power spectrum in the temporal and spatial mode 1 at a frequency of 12 was reached at the significant level 99.5 % with the F value of 339.2 and 29.25, respectively. The variance of power spectrum for 7 months was also reached at the significant level 95 % with the F value of 4.03.

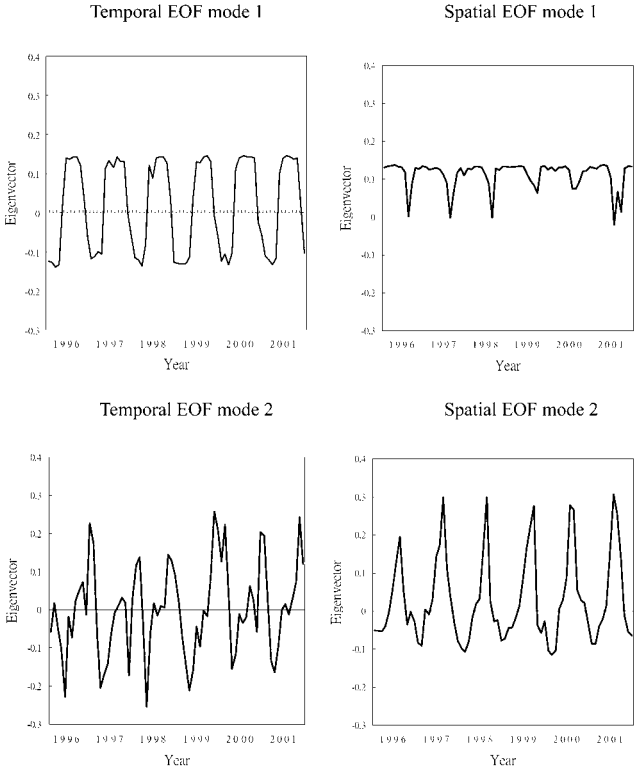

Fig. 4. Time series of the temporal and spatial EOF mode 1 & 2 eigenvectors.

DISCUSSIONS

Remotely sensed infrared imagery of sea surface temperature has been increasingly utilized to study, assess, and characterize surface dynamic properties of ocean current. In this study, the NOAA/AVHRR sea surface temperature images with the EOF method were

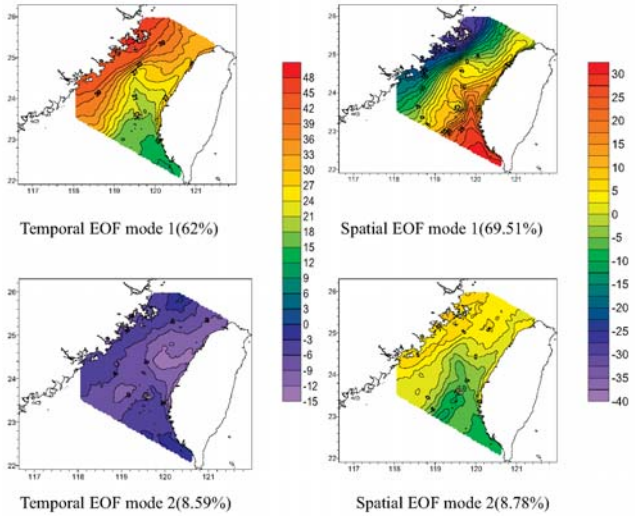

Fig. 5. Temporal and spatial amplitude images for the time-series EOF analysis of the Taiwan Strait.

examined to extract surface features over the Taiwan Strait. The result indicated the heavily dominant mode of spatial variance for Taiwan Strait to be consistent with a quasi-permanent front at Chang-Yuen Ridge in winter and associated strong temperature contrast from the Kuroshio branch or South China Sea Warm Current. The South China Sea Warm Current was over the Peng-Hu channel following to the 60 to 100-m depth contour. This was similar to the result of Jan *et al*. [9] who examined the seasonal variation of the circulation in Taiwan Strait. They indicate a warm tongue may protrude northward from the northern end of the Peng-Hu channel when the northeast monsoon temporally weakened or diminished. They also thought the combination of monsoon and topography forcing leads to the winter blocking of northward current and spring renewal of northward intrusion, and fall emergence of China Coastal Current.

The power spectrum contained a large peak at a period of 12 months (Figure 6). They could properly represent a physical process, as the variance analysis was reached at the significantly level 99.5%. It also suggested that the amplitude functions showed this signal to be consistent with the annual heating balance and the formation of oceanic front boundary at the Chang-yuen Ridge. Keiner and Yan [11] think that the first dominant mode in the decomposition after the temporal mean has been removed is associated with the seasonal heating signal. From the results of EOF, the amplitude patterns and the eigenvalues in time and space were similar to each other. These first two spatial amplitude modes of temporal and spatial variance accounted for 70.59% and 78.3% of the SST variance, respectively. The first EOF mode, which resembled the mean of all images, showed a crescent-shaped front located near the Chang-Yuen Ridge where a cool tongue extending from the China coastal waters was distinguishable with the warm current. It suggested that the isopleths line of spatial amplitude zero might be the boundary index of the China coastal waters and the South China Warm waters (Fig. 4). This result of the crescent-shaped front was similar to that of Jan *et al* [8] who find a zonal oceanic front develops over the Chang-Yuen Ridge in winter. They also indicate that the sea surface temperature patterns in Taiwan Strait are true of modes whose strong temporal oscillation creates strong spatial gradients. Fan and Yu [3] suggest that the northward warm and saline water originally from Kuroshio branch current is blocked at the southern side of the Chang-Yuen Ridge in winter. Otherwise, the power spectrum also showed a weak peak at a period of 7 months in spatial EOF mode 1 (Fig. 6). It indicated that the EOF function was difficult to extract the seasonal SST variation of Taiwan Strait by using the monthly mean SST imageries, as the hydrographic characteristics of ocean color (i.e. chlorophyll pigment concentration) was more significant than that of SST in the waters off southwestern Taiwan during summertime (Figure 7).

It was interesting to note that the spatial amplitude patterns of spatial EOF mode 2 had positive values in the coastal waters of Mainland China. And spatial amplitudes of the deeper waters up to the middle of the strait remained near zero or negative values. This suggested that the near-zero spatial amplitude occur-

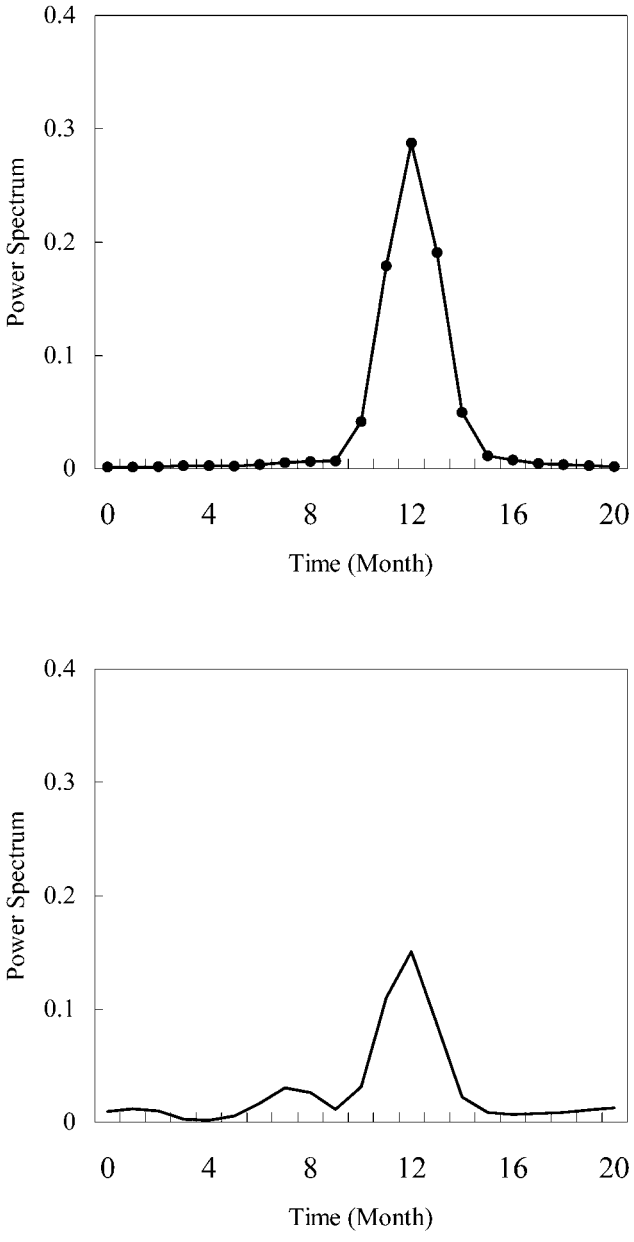

Fig. 6. Power spectrum of eigenvectors in temporal (upper) and spatial (lower) EOF mode 1 of Figure 4, respectively.

ring in the Chang-Yuen Ridge illustrated that the SST in this area did not oscillate with the second mode. This was similar to that of Jan *et al.* [7, 8] who thought a wave-like density structure was formed in the central part of the Taiwan Strait. However, the monthly temporal and spatial distribution of wave-like structure in SST did not remain constant in January and February of 1999 and 2000 (Figure 8). As the strength of Kuroshio intrusion was extended to the west of longitude 120 E, the crescentic-shaped structure weakened and moved near to the waters off the Peng-Hu Islands. And the counter current of Kuroshio was formed at the east of longitude 120 E, the highlight of wave-like structure strengthened and moved over to the waters of Chang-Yuen Ridge. This result suggested that the variance of SST patterns in Taiwan Strait might be consider a interaction mechanism with the intrusion of the Kuroshio current in the southern East China Sea. It was similar to the result of Tang *et al.* [20] who examined the flow pattern north of Taiwan and the movement of the Kuroshio. Though the impact of the Taiwan Strait outflow on the Kuroshio flow pattern north of Taiwan was not negligible, it was not as great as the impact of the Kuroshio, and thus, the intrusion of the Kuroshio strongly influenced the Taiwan Strait outflow [20].

From the AVHRR satellite imageries, it also displayed a cool water plume extending from the Peng-Hu Islands to the Formosa Banks in summer (Figure 2). The formation of this cool water plume was attributable to the upwelling. However, it was hard to explain this phenomenon in this study. This was caused by the data used, as the southern boundary of Taiwan Strait defined from the southern tips of Taiwan to the Tung-Sun Island was crossed over the upwelling zone (Figures 1 & 2). For this, a studied setting sample of satellite imagery in this upwelling zone was suggested to examine the hydrographic patterns in the future.

CONCLUSION

Satellite imagery provided high-resolution data on large-scale hydrographic pattern which was unobtainable using traditional field sampling strategies. We showed that EOF might be useful for defining modes of SST variation in the Taiwan Strait. The most important of these modes suggested that they might be closely related to the processes maintaining the heat balance of the ocean surface. It also provided value information into the annual pattern of SST variability. In this strait the annual cycle predominated, accounting 70.6~78.3% of the SST variance. However, Gallaudet and Simpson [5] suggest that the interpretation of EOF modes still requires a considerable amount of physical insight, and comparison with concurrent *in-situ* data [11]. But this EOF method produced excellent results for decomposing mode that vary largely in space or time alone, as *in-*

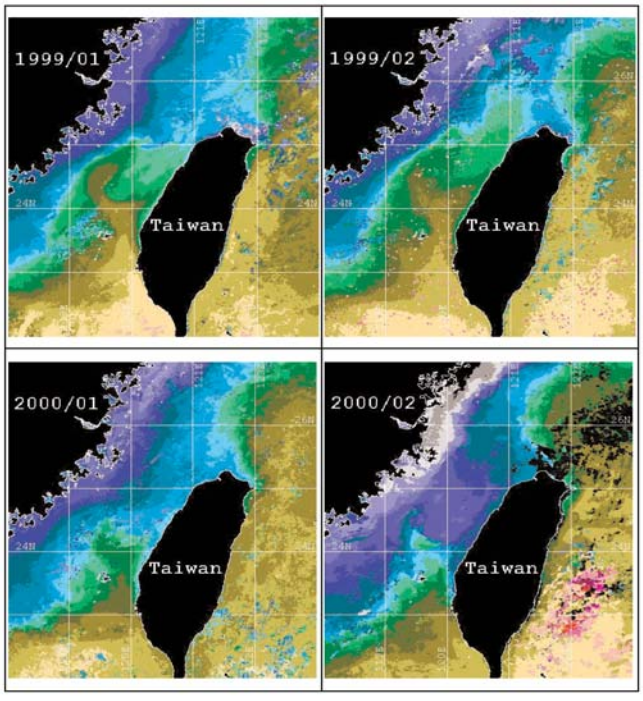

Fig. 7. The satellite imageries of monthly mean SST (upper) and Chlorophyll pigment concentration (lower) in August of 1998 and 1999.

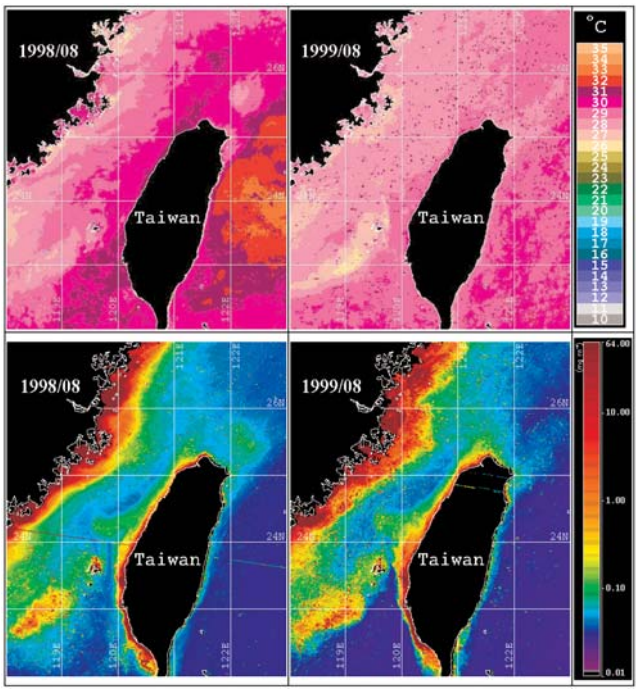

Fig. 8. The monthly mean SST satellite imageries in January and February of 1999 and 2000.

situ observation was still not available. In the future, the time-series weekly or daily SST and ocean color satellite imageries with full resolution should be allowed for finer detail in the analysis. A longer time-series will also provide more insight into the seasonal or micro-scale variability of the SST in Taiwan Strait.

ACKNOWLEDGEMENT

We would like to express our appreciation to Mr. I.M. Chen and M.S. Chou for their assistance on SST imageries extracted and the EOF analysis, respectively. The study was financially supported by the National Science Council (NSC 89-2611-M-019-02-04-op4 and NSC 89-2119-M019-004) of the Republic of China (R.O.C).

REFERENCES

1. Cole, J., "Environmental Conditions, Satellite Imagery, and Clupeid Recruitment in the Northern Benguela Upwelling System," *Fish. Oceanogr.*, Vol. 8, No. 1, pp. 25-38 (1999).
2. Emery, W.J., Thomas, A.C., Collins, M.J., Crawford, W.R., and Mackas, D.L., "An Objective Method for Computing Advective Surface Velocities from Sequential Infrared Satellite Images," *J. Geophys. Res.*, Vol. 91, No. C11, pp. 12865-12878 (1986).
3. Fan, K.L. and Yu, C.Y., "A Study of Water Masses in the Seas of Southernmost Taiwan," *Acta Oceanogr. Taiwanica*, Vol. 12, pp. 94-111 (1981).
4. Fielder, P.C. and Bernard, H.J., "Tuna Aggregation and Feeding Near Fronts Observed in Satellite Imagery," *Conti. Shelf Res.*, Vol. 7, pp. 871-881 (1987).
5. Galladudet, T.C. and Simpson, J.J., "An Empirical Orthogonal Function Analysis of Remotely Sensed Sea Surface Temperature Variability and its Relation to Interior Oceanic Processes off Baja California," *Remote sens. Environ.*, Vol. 47, pp. 375-389 (1994).
6. Huang, W.G., Cracknell, A.P., Vaughan, R.A., and Davies, P.A., "A Satellite and Field View of the Irish Shelf Front," *Conti. Shelf Res.*, Vol. 11, No. 6, pp. 543-562 (1991).
7. Jan, S., Chen, C.S., and Wang, J., "A Numerical Study on Currents in the Taiwan Strait During Summertime," *La Mer.*, Vol. 32, pp. 225-234 (1994).
8. Jan, S., Chen, C.S., and Wang, J., "A Numerical Study on Currents in the Taiwan Strait During Winter," *TAO*, Vol. 9, No. 4, pp. 615-632 (1998).
9. Jan, S., Wang, J., Chern, C.S., and Chao, S.Y., "Seasonal Variation of the Circulation in the Taiwan Strait," *J. Mari. Sys.*, Vol. 35, pp. 249-268 (2002).
10. Kahru, M., Hakansson, B., and Rud, O., "Distributions of the Sea-surface Temperature Fronts in the Baltic Sea as Derived from Satellite Imagery," *Conti. Shelf Res.*, Vol. 15, No. 6, pp. 663-679 (1995).
11. Keiner, L.E. and Yan, X.H., "Empirical Orthogonal Function Analysis of Sea Surface Temperature Patterns in Delaware Bay," *IEEE Transactions on Geoscience and remote sensing*, Vol. 35, No. 5, pp. 1299-1306 (1997).
12. Kelly, K.A., "The Influence of Winds and Topography on the Sea Surface Temperature Patterns Over the Northern California Slope," *J. Geophys. Res.*, Vol. 90, No. C6, pp. 11783-11798 (1985).
13. Kubota, M., "A New Cloud Detection Algorithm for Nighttime AVHRR/HRPT Data," *J. Oceanogr.*, Vol. 50, pp. 31-41 (1994).
14. Lagerloef, G.S.E. and Bernstein, R.L., "Empirical Orthogonal Function Analysis of Advanced Very High Resolution Radiometer Surface Temperature Patterns in Santa Barbara Channel," *J. Geo. Res.*, Vol. 93, No. C6, pp. 6863-6873 (1988).
15. Liao, C.H., Lee, K.T., Lee, M.A., and Lu, H.J., "Oceanographic Conditions and Surface Layer Biomass Distribution Characteristics in the Waters of Northern Taiwan," *J. Fish. Soc. Taiwan*, Vol. 24, No. 4, pp. 283-297 (1997).
16. Paden, C.A., Abbott, M.R., and Winant, C.D., "Tidal and Atmospheric Forcing of the Upper Ocean in the Gulf of California, 1: Sea Surface Temperature Variability," *J. Geophys. Res.*, Vol. 96, No. C10, pp. 18337-18359 (1991).
17. Power, J.H. and MayJr, L.N., "Satellite Observed Sea-surface Temperatures and Yellow Fin Tuna Catch and Effort in Gulf of Mexico," *Fish. Bull.*, Vol. 89, pp. 429-439 (1991).
18. Simpson, J.J. and Humphrey, C., "An Automated Cloud Screening Algorithm for Daytime Advanced Very High Resolution Radiometer Imagery," *J. Geophys. Res.*, Vol. 95, No. C8, pp. 13459-13481 (1990).
19. Stumpf, H.G. and Rao, P.K., "Evolution of Gulf Stream Eddies as Seen in Satellite Infrared Imagery," *J. Phys. Oceanogr.*, Vol. 5, pp. 388-393 (1975).
20. Tang, T.Y, Tai, J.H., and Yang, Y.J., "The Flow Pattern North of Taiwan and the Migration of the Kuroshio," *Conti. Shelf Res.*, Vol. 20, pp. 349-371 (2000).
21. Tseng, C.T., Lin, C.Y., Chen, S.C., and Shyu, C.Z., "Temporal and Spatial Variation of Sea Surface Temperature in the East China Sea," *Conti. Shelf Res.*, Vol. 29, pp. 373-387 (2000).